Journal of Alloys and Compounds 509 (2011) 1111–1114

Contents lists available at ScienceDirect

Journal of Alloys and Compounds

journal homepage: www.elsevier.com/locate/jallcom

Magnetic and magnetocaloric properties in melt-spun and annealed $Ni_{42.7}Mn_{40.8}Co_{5.2}Sn_{11.3}$ ribbons

S.C. Ma[a], Q.Q. Cao[a,*], H.C. Xuan[a], C.L. Zhang[a,b], L.J. Shen[a], D.H. Wang[a], Y.W. Du[a]

[a] National Laboratory of Solid State Microstructures and Key Laboratory of Nanomaterials for Jiang Su Province, Nanjing University, Nanjing 210093, People's Republic of China
[b] School of Science, Jiangnan University, Wuxi 214122, People's Republic of China

ARTICLE INFO

Article history:
Received 5 August 2010
Received in revised form
26 September 2010
Accepted 29 September 2010
Available online 8 October 2010

Keywords:
Ferromagnetic shape memory alloys
Melt-spun and annealed ribbons
Magnetocaloric property
Effective refrigerant capacities

ABSTRACT

The $Ni_{42.7}Mn_{40.8}Co_{5.2}Sn_{11.3}$ ribbons were prepared by melt spinning. After heat treatment, the martensitic transformation temperature and Curie temperature of austenite of the annealed ribbons increased remarkably. Inverse and direct magnetocaloric properties were investigated in the melt-spun and annealed ribbons. The effective refrigerant capacities for these ribbons were discussed in this paper.

1. Introduction

Magnetocaloric effect (MCE) has been a research focus during the past several decades which is ascribed to the fact that magnetic refrigeration based on it has been regarded as a promising alternative technique for its high efficiency and environmental friendliness [1–3]. It is well known that the key of magnetic refrigeration is searching for the magnetic materials exhibiting large MCE in the relatively low field. In this context, more and more attention have been paid to the materials undergoing the first-order magnetic phase transition (FOMT), such as $Gd_5Si_2Ge_2$ [4], $MnFeP_{0.45}As_{0.55}$ [3], $LaFe_{11.4}Si_{1.6}$ [5], and $Mn_{1.9-x}Ni_xGe$ [6], *etc.* Among them, the Ni–Mn based ferromagnetic shape memory alloys (FSMAs) Ni–Mn–X (X = Ga, In, Sn, and Sb) have been received increasing attention because of several noteworthy characteristics, for instance, large magnetic field-induced-strain, relatively cheap raw materials, and adjustable phase transition temperature [7–21]. After the discovery of large MCE in off-stoichiometric Ni–Mn based FSMAs [8,9], the effect of partial substitution of Co for Ni or Mn in these alloys on their magnetic properties and MCE have been studied [10–12]. In the previous reports, it was suggested that Co substitution induced the Mn moments align in a ferromagnetic ordering, giving rise to the magnetization in the austenitic phase [10,11]. Gao et al. also pointed out that the addition of Co notably enhanced the magnetization discrepancy ΔM across the martensitic transformation (MT) in $Ni_{43}Mn_{46-x}Co_xSn_{11}$ alloys, because the magnetization of austenitic phase was significantly increased while that of martensitic state kept nearly unchanged [12]. Large MCE originated mainly from this large ΔM makes Ni–Mn–Co–Sn alloys potential refrigerant [11,12].

Up to now, most investigation of Ni–Mn based FSMAs has focused on bulk polycrystalline alloys. Very recently, homogeneous Ni–Mn–X ribbons were produced using the rapid solidification method by melt spinning, which was proved to be a very effective way to synthesize highly textured polycrystalline ribbons avoiding or reducing annealing time [13–19]. The microstructure, MT, magnetic properties, and MCE of these ribbons were investigated consequently [13–19]. As far as we know, however, there are few reports about the Ni–Mn–Co–Sn ribbons. In the present paper, we prepared Ni–Mn–Co–Sn ribbons by rapid quenching and investigated MT and MCE for the melt-spun and annealed ribbons.

2. Experimental

Ni–Mn–Co–Sn ribbons were prepared by melt-spinning the as-cast Ni–Mn–Co–Sn alloy in argon atmosphere at a surface velocity of 10 ms^{-1}. Some of the melt-spun ribbons were sealed in evacuated quartz tubes and annealed at 1123 K for 10 min with a subsequent quench in cool water. The exact composition of the ribbon is determined as $Ni_{42.7}Mn_{40.8}Co_{5.2}Sn_{11.3}$, which is estimated by X-ray energy dispersive spectroscopy (EDS) microanalysis. Thermal behavior was studied using a differential scanning calorimeter (DSC) with the heating and cooling rates of 10 K/min. The magnetization measurements were carried out using a vibration sample magnetometer (7300, Lakeshore) under a magnetic field up to 10 kOe. The

* Corresponding author. Tel.: +86 25 83594588; fax: +86 25 83595535.
E-mail address: qqcao@nju.edu.cn (Q.Q. Cao).

0925-8388/$ – see front matter © 2010 Elsevier B.V. All rights reserved.
doi:10.1016/j.jallcom.2010.09.205

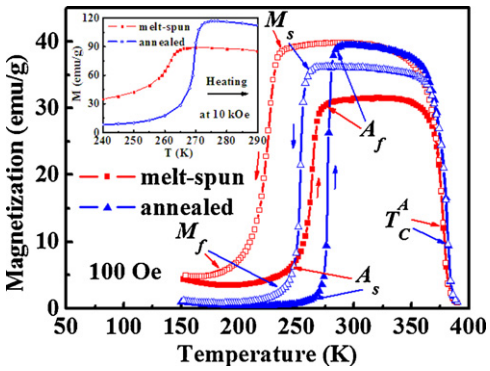

Fig. 1. Temperature dependence of the magnetization for the melt-spun and annealed $Ni_{42.7}Mn_{40.8}Co_{5.2}Sn_{11.3}$ ribbons on heating (solid symbols) and cooling (open symbols) under a field of 100 Oe. M_s and M_f denote the starting and finishing temperatures of the martensitic transformation, A_s and A_f denote the starting and finishing temperatures of the reverse transformation, and T_C^A is the Curie temperature of austenite. The inset presents thermomagnetic curves for these ribbons under a field of 10 kOe around MT.

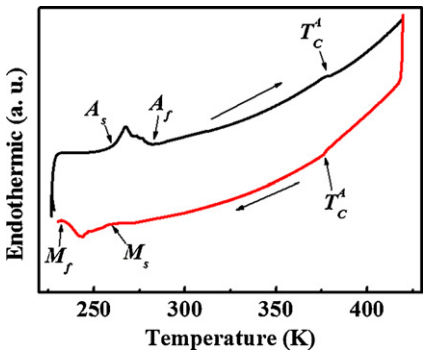

Fig. 2. DSC curves for the annealed $Ni_{42.7}Mn_{40.8}Co_{5.2}Sn_{11.3}$ ribbons on cooling and heating.

applied magnetic field was perpendicular to the ribbon axis (along the ribbon's surface).

3. Results and discussions

The thermomagnetic M (T) curves for the melt-spun and annealed $Ni_{42.7}Mn_{40.8}Co_{5.2}Sn_{11.3}$ ribbons on heating and cooling under a field of 100 Oe are shown in Fig. 1. It can be seen that these two ribbons show similar thermomagnetic behavior. On heating, a reverse MT from the weak-magnetic martensitic phase to ferromagnetic parent phase is first observed with an abrupt jump of the magnetization, revealing a strong correlation between the magnetism and structure in these ribbons. Further increasing temperature leads to a ferromagnetic–paramagnetic transition occurring at the Curie temperature of austenite T_C^A. After annealing, the reverse MT temperature T_M (forward MT temperature T_A) and T_C^A, defined as the temperatures where dM/dT are maximum, increase remarkably. These results agree well with that of $Ni_{44.1}Mn_{44.2}Sn_{11.7}$ ribbons, which would be ascribed to the change of Mn–Mn distance induced by the stress and structural relaxations [16]. The characteristic temperatures of these ribbons (austenitic start A_s and finish temperatures A_f, martensitic start M_s and finish temperatures M_f) around MT are denoted in Fig. 1. Note that these temperatures of annealed ribbons are near room temperature, which is of importance for practical application. It can also be observed that the magnetization of annealed ribbons increases more sharply than that of melt-spun ones around MT and ΔM between martensitic and austenitic phases increases remarkably in the annealed ribbons. The narrower temperature interval where MT occurs and the enhanced ΔM suggest a larger near-room-temperature ΔS_M in the annealed ribbons. Moreover, the thermal hysteresis between the cooling and heating processes decreases evidently after annealing. The partly removed defects and released internal stresses resulting from relatively larger grains by annealing would be responsible for the reduced hysteresis in the annealed ribbons [16,18]. The inset of Fig. 1 shows the M (T) curves on heating measured under the field of 10 kOe. Comparing with M (T) curves at 100 Oe, T_M shifts to the lower temperature obviously due to the fact that the application of magnetic field would induce MT occurring at lower temperature [12,18,20].

Fig. 2 shows the DSC cooling and heating curves for the annealed $Ni_{42.7}Mn_{40.8}Co_{5.2}Sn_{11.3}$ ribbons in the temperature range between 220 and 430 K. Large exothermic and endothermic peaks, corresponding to the forward and reverse MTs, respectively, are observed. The characteristic transition temperatures obtained from DSC curves are in agreement with that obtained from thermomagnetic measurement. The thermal hysteresis of about 24 K is observed. In the higher temperature range, small exothermic and endothermic peaks are detected around T_C^A on cooling and heating curves, respectively.

The selected magnetization isotherms for the melt-spun and annealed ribbons around MT and T_C^A are shown in Fig. 3(a)–(d). For clarity, only some selected M–H hysteresis loops around MT are shown in Fig. 3(a) and (b). As presented in Fig. 3(a) and (b), the magnetization of parent phase increases markedly after annealing. As we know, the atom site in melt-spun ribbons may be not too stable, since they are prepared by the quick transition from the liquid to the solid state, and do not take up an equilibrium position, in which they would have lower energy [22]. After annealing, the melt-spun ribbons would undergo structural and stress relaxations. These relaxations, involving atomic rearrangements, may modify the atom site slightly, resulting in the change of Mn–Mn distance [22]. Since the magnetic properties of Ni–Mn based FSMAs are very sensitive to the Mn–Mn distance [23,24], the magnetization of annealed ribbons would change correspondingly. As mentioned above, the jump of magnetization around T_M increases remarkably after annealing. The increased ΔM suggests that the magnetic field-induced MT would overcome a large potential barrier to occur between martensite phase and austenite phase in the annealed ribbons. Therefore, a sharp metamagnetic transition with a large magnetic hysteresis is observed in the annealed ribbons, as shown in Fig. 3(b). On the other hand, as indicated in Fig. 3(c) and (d), the magnetization of austenite for the annealed ribbons is larger than that of melt-spun ones, but no metamagnetic behavior can be observed.

The values of ΔS_M as a function of temperature around MT and T_C^A for these ribbons are calculated from the isothermal magnetization curves. As shown in Fig. 4 and its inset, ΔS_M increases obviously after annealing. The detailed values of ΔS_M for these ribbons are listed in Table 1. This increment would be ascribed to the more abrupt change of magnetization and the larger ΔM around T_M and T_C^A for the annealed ribbons as mentioned above.

Besides ΔS_M, the refrigerant capacity (RC) is also an important parameter to evaluate MCE. RC values are usually determined by numerically integrating the area under the ΔS_M (T) curves, the integration limits using the temperature at the full width half maximum of the ΔS_M peak [25]. So the temperature interval is generally regarded as the useful working temperature range of the materials. Note that, in the FOMT materials, the hysteretic losses around the phase transition should be taken into account in the evaluation of RC. Here the hysteretic losses at different temperatures are obtained by calculating the area between the magnetizing and demagnetizing M (H) curves shown in Fig. 3 [14,15,19,21]. Hysteretic losses at 10 kOe as a function of temperature for the

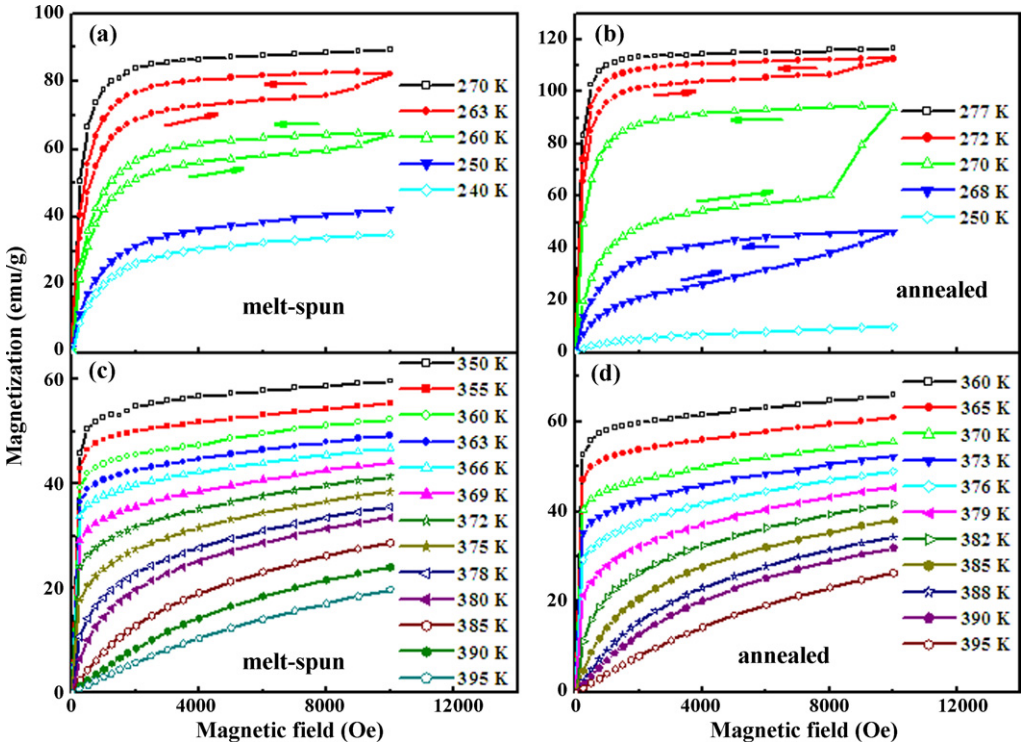

Fig. 3. Magnetization isotherms on heating for the melt-spun [(a) and (c)] and annealed [(b) and (d)] $Ni_{42.7}Mn_{40.8}Co_{5.2}Sn_{11.3}$ ribbons measured around MT and T_C^A.

Table 1
Maximum of magnetic entropy change ΔS_M^{max}, useful working temperature range δT_{FWHM}, refrigerant capacity *RC*, average hysteretic losses, and effective refrigerant capacity RC_{eff} values for the melt-spun and annealed $Ni_{42.7}Mn_{40.8}Co_{5.2}Sn_{11.3}$ ribbons around MT and T_C^A for a field change of 10 kOe.

Samples	Phase transition around	ΔS_M^{max} (J kg^{-1} K^{-1})	T_{cold} (K)	T_{hot} (K)	δT_{FWHM} (K)	*RC* (J kg^{-1})	Average hysteretic losses (J kg^{-1})	RC_{eff} (J kg^{-1})
Melt-spun	MT	6.8	259	274	15	24	5	19
	T_C^A	−1.3	319	394	75	67	0	67
Annealed	MT	32.8	269	271	2	44	25	19
	T_C^A	−1.6	310	394	84	91	0	91

melt-spun and annealed ribbons are presented in Fig. 5. The average hysteretic losses for these ribbons are calculated by integrating the area under the curves of hysteresis losses versus temperature using the same temperature range as the calculation of *RC* as the integration limits [14,15,19,21]. Therefore, the effective *RC* is evaluated by subtracting the average hysteresis loss from *RC* for these ribbons. The values of *RC*, average hysteretic losses and the effective *RC* (RC_{eff}) for these ribbons are also listed in Table 1. Around MT, although *RC* of the annealed ribbons is larger than that of melt-spun ones, the values of RC_{eff} for both melt-spun and annealed ribbons retain almost unchanged (19 J kg^{-1}), which would be ascribed to the larger hysteretic losses associated with the more notable

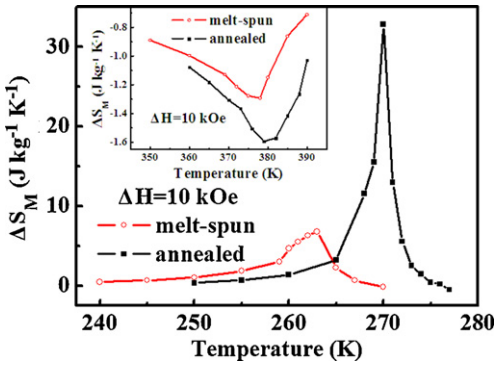

Fig. 4. Magnetic entropy change as a function of temperature for the melt-spun and annealed $Ni_{42.7}Mn_{40.8}Co_{5.2}Sn_{11.3}$ ribbons around MT in the field of 10 kOe. Inset: temperature dependence of the magnetic entropy change around T_C^A for these ribbons.

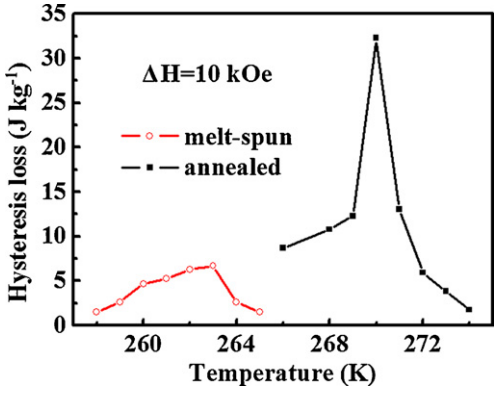

Fig. 5. Variation of the hysteresis losses for the melt-spun and annealed $Ni_{42.7}Mn_{40.8}Co_{5.2}Sn_{11.3}$ ribbons around MT versus temperature for a field change of 10 kOe.

field-induced metamagnetic transition in the annealed ribbons discussed above [14,15]. But in the vicinity of T_C^A for these ribbons, the average hysteretic losses are zero due to the character of the second-order phase transition, and therefore, the enhanced RC_{eff} is obtained after annealing. As mentioned above, the value of the ΔS_M around MT is larger than that around T_C^A, but in the case of RC_{eff}, an opposite result is obtained. It should be pointed out that RC_{eff} values around T_C^A for these ribbons, especially the annealed ones, are comparable to, or even larger than some other magnetocaloric materials considering the same conditions, such as the melt-spun Ni–Mn–Sn ribbons (46 J Kg^{-1}, ΔH = 20 kOe) [14], the melt-spun Ni–Mn–Ga ribbons (45.5 J Kg^{-1}, ΔH = 20 kOe) [19], and Ni–Co–Mn–Fe–Ga alloy (70 J Kg^{-1}, ΔH = 50 kOe) [21].

4. Conclusions

Effects of annealing on the magnetic and magnetocaloric properties in $Ni_{42.7}Mn_{40.8}Co_{5.2}Sn_{11.3}$ ribbons have been investigated. T_M and T_C^A of the annealed ribbons increase obviously, owing to the stress and structural relaxations. The thermal hysteresis decreases for the annealed ribbons due to the partially removed defects and released internal stress resulting from the relatively larger grains after annealing. The enhanced magnetization and obvious metamagnetic behavior can be observed in the annealed ribbons. Large near-room-temperature MCE are observed in these ribbons. The values of ΔS_M around MT and T_C^A of the annealed ribbons are larger than those of melt-spun ones. However, RC_{eff} around MT is almost unchanged for these ribbons, owing to the larger hysteretic losses associated with the more evident field-induced metamagnetic transition in the annealed ribbons. Around T_C^A, RC_{eff} increases remarkably after heat treatment and is much larger than that around MT.

Acknowledgements

This work is supported by the National Basic Research Program of China (2005CB623605), National Natural Science Foundation of China (50701022 and 50831006) and the Program for New Century Excellent Talents of China (NCET-08-0278).

References

[1] J. Glanz, Science 279 (1998) 2045.
[2] S. Fujieda, A. Fujita, K. Fukamichi, Appl. Phys. Lett. 81 (2002) 1276–1278.
[3] O. Tegus, E. Brück, K.H.J. Buschow, F.R. de Boer, Nature (London) 415 (2002) 150–152.
[4] V.K. Pecharsky, K.A. Gschneidner Jr., Phys. Rev. Lett. 78 (1997) 4494–4497.
[5] F.X. Hu, B.G. Shen, J.R. Sun, Z.H. Cheng, G.H. Rao, X.X. Zhang, Appl. Phys. Lett. 78 (2001) 3675–3677.
[6] C.L. Zhang, D.H. Wang, Q.Q. Cao, Z.D. Han, H.C. Xuan, Y.W. Du, Appl. Phys. Lett. 93 (2008) 122505.
[7] R. Kainuma, Y. Imano, W. Ito, Y. Sutou, H. Morito, S. Okamoto, O. Kitakami, K. Oikawa, A. Fujita, T. Kanomota, K. Ishida, Nature (London) 439 (2006) 957–960.
[8] T. Krenke, E. Duman, M. Acet, E.F. Wassermann, X. Moya, L. Manosa, A. Planes, Nat. Mater. 4 (2005) 450–454.
[9] Z.D. Han, D.H. Wang, C.L. Zhang, H.C. Xuan, B.X. Gu, Y.W. Du, Appl. Phys. Lett. 90 (2007) 042507.
[10] L. Ma, H.W. Zhang, S.Y. Yu, Z.Y. Zhu, J.L. Chen, G.H. Wu, H.Y. Liu, J.P. Qu, Y.X. Li, Appl. Phys. Lett. 92 (2008) 032509.
[11] Z.D. Han, D.H. Wang, B. Qian, J.F. Feng, X.F. Jiang, Y.W. Du, Jpn. J. Appl. Phys. Part 1 49 (2010) 010211.
[12] B. Gao, F.X. Hu, J. Shen, J. Wang, J.R. Sun, B.G. Shen, J. Magn. Magn. Mater. 321 (2009) 2571–2574.
[13] B. Hernando, J.L. Sánchez Llamazares, J.D. Santos, Ll. Escoda, J.J. Suñol, R. Varga, D. Baldomir, D. Serantes, Appl. Phys. Lett. 92 (2008) 042504.
[14] B. Hernando, J.L. Sánchez Llamazares, J.D. Santos, V.M. Prida, D. Baldomir, D. Serantes, R. Varga, J. González, Appl. Phys. Lett. 92 (2008) 132507.
[15] B. Hernando, J.L. Sánchez Llamazares, V.M. Prida, D. Baldomir, D. Serantes, M. Ilyn, J. González, Appl. Phys. Lett. 94 (2009) 222502.
[16] H.C. Xuan, K.X. Xie, D.H. Wang, Z.D. Han, C.L. Zhang, B.X. Gu, Y.W. Du, Appl. Phys. Lett. 92 (2008) 242506.
[17] J. Liu, N. Scheerbaum, J. Lyubina, O. Gutfleisch, Appl. Phys. Lett. 93 (2008) 102512.
[18] J. Liu, T.G. Woodcock, N. Scheerbaum, O. Gutfleisch, Acta Mater. 57 (2009) 4911–4920.
[19] N.V. Rama Rao, R. Gopalan, V. Chandrasekaran, K.G. Suresh, J. Alloys Compd. 478 (2009) 59–62.
[20] F.X. Hu, J. Wang, J. Shen, B. Gao, J.R. Sun, B.G. Shen, J. Appl. Phys. 105 (2009) 07A940.
[21] A.K. Pathak, I. Dubenko, H.E. Karaca, S. Stadler, N. Ali1, Appl. Phys. Lett. 97 (2010) 062505.
[22] D.H. Wang, K. Peng, B.X. Gu, Z.D. Han, S.L. Tang, W. Qin, Y.W. Du, J. Alloys Compd. 358 (2003) 312–315.
[23] P.J. Brown, A.P. Gandy, K. Ishida, R. Kainuma, T. Kanomata, K.U. Neumann, K. Oikawa, B. Ouladdiaf, K.R.A. Ziebeck, J. Phys.: Condens. Matter 18 (2006) 2249–2259.
[24] E. Sasioğlu, L.M. Sandratskii, P. Bruno, Phys. Rev. B 71 (2005) 214412.
[25] K.A. Gschneidner Jr., V.K. Pecharsky, A.O. Pecharsky, C.B. Zimm, Mater. Sci. Forum 315–317 (1999) 69–76.